Journal of Power Sources 242 (2013) 838–843

Contents lists available at SciVerse ScienceDirect

Journal of Power Sources

journal homepage: www.elsevier.com/locate/jpowsour

Arrayed titanium dioxide shells architecture as anode of lithium ion microbattery

Jianfei Lei [a,b], Weishan Li [a,c,d,*], Xiaoping Li [a,c,d], Lizhen Zeng [a]

[a] School of Chemistry and Environment, South China Normal University, Guangzhou 510006, China
[b] School of Physics and Engineering, Henan University of Science and Technology, Luoyang 471023, China
[c] Key Laboratory of Electrochemical Technology on Energy Storage and Power Generation of Guangdong Higher Education Institutes, South China Normal University, Guangzhou 510006, China
[d] Engineering Research Center of Materials and Technology for Electrochemical Energy Storage (Ministry of Education), South China Normal University, Guangzhou 510006, China

HIGHLIGHTS

- TiO_2-NCs electrode was constructed as anode of lithium ion microbattery.
- Hierarchical structure of TiO_2 with {001} facets yields good rate capability and cycle stability.
- Highly mesoporous and microporous nature contributes to rate performance.

GRAPHICAL ABSTRACT

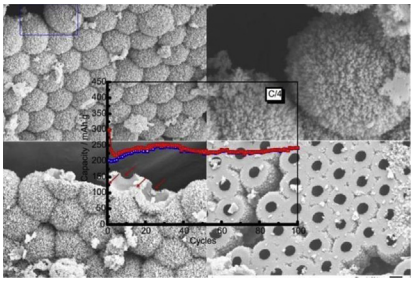

ARTICLE INFO

Article history:
Received 11 April 2013
Received in revised form
26 May 2013
Accepted 28 May 2013
Available online 10 June 2013

Keywords:
Titanium dioxide
Template
Lithium ion battery
Array

ABSTRACT

TiO_2 nanocones (TiO_2-NCs) are constructed into arrayed spherical shells through a liquid-phase deposition reaction with polymer template, to improve the performance of TiO_2 as anode of lithium ion microbattery. The morphology and structure characterizations indicate that TiO_2 grows into nanocones with exposed {001} facets and is self-assembled into mesoporous structure. Meanwhile, macroporous channels are formed among the arrayed shells. Electrochemical measurements demonstrate that the TiO_2-NCs reveal excellent performance in terms of improved lithium storage property and rate capability. The improved performance can be ascribed to the channel structure for the convenience of ionic transportation and the high-energy facets for the improvement of ionic reactivity.

1. Introduction

Lithium ion batteries are today used for a wide range of applications in micro-device fields (MDF) and hybrid electric vehicles (HEV) [1–8]. In the MDF, miniaturization is important to make a high energy and power on a small footprint area, which requires nanostructured materials for batteries. Lithium ion microbattery is a miniaturized power source with thin-film structured electrodes to miniaturize essentially the geometry of standard batteries, and many nanostructured materials [9–17], especially carbon-based materials, have been developed to be used as the negative materials for this microbattery. Unfortunately, the cycle stability of traditional carbon materials is poor and the formation of the solid electrolyte interphase (SEI) on carbon materials due to its low lithium inserted potential is a serious threat to the safety of the battery [18–20].

* Corresponding author. School of Chemistry and Environment, South China Normal University, Guangzhou 510006, China.
E-mail address: liwsh@scnu.edu.cn (W. Li).

0378-7753/$ – see front matter © 2013 Elsevier B.V. All rights reserved.
http://dx.doi.org/10.1016/j.jpowsour.2013.05.166

Titanium-containing oxides, such as TiO_2 and $Li_4Ti_5O_{12}$, have better structure stability and higher lithium insertion potential (~1.5 V *vs.* Li^+/Li) than carbon materials and thus provide lithium ion batteries with excellent cycle performance [21,22]. Compared with other titanium oxides, anatase TiO_2 exhibits superior properties, including the simplicity for synthesizing with nanostructure and high lithium storage capacity [23]. Anatase TiO_2 with a tetragonal crystal structure has been widely investigated and a large number of nanostructured anatase TiO_2 materials have been constructed for photocatalysis, gas sensor and electrochemical energy conversion and storage devices [7,11,13,24–27]. Earlier studies demonstrated that highly-active {001} facets of anatase TiO_2 exhibit superior photocatalytic activity when normalized by the surface area [28–30], and recent studies showed that these facets also provided unusual opportunities for electrochemical energy storage [31,32]. To exploit the activity of anatase TiO_2 with exposed {001} facets [23], a series of studies have been performed for the synthesis of sheet-like TiO_2 (TiO_2 nanosheet) [33–36]. However, the formation of the nanosheet should be in a special reactor (autoclave) and the final product is usually as powders, which limit its applications.

In our previous report, we prepared cone-like TiO_2 (TiO_2-NCs) with exposed {001} facets through a convenient process and then assembled them into hollow spheres with polymer template [37]. We used the TiO_2-NCs as the support of tin oxide nanoparticles to develop a novel negative composite for lithium ion battery. In this composite, the high Li^+-transport dynamics of titanate hollow spheres (TiO_2) and high capacity of tin oxide (SnO_2) were intimately integrated into a hierarchical architecture of nanocones, while the unique spatial arrangement of SnO_2 component in the nano-cavities effectively accommodates the volume change during lithiation/de-lithiation, hence rendering the composite stable cycling life. The developed TiO_2-NCs exhibits enhanced lithium storage capacity compared to the TiO_2 nanospindles [25] and improved rate capability compared to the porous TiO_2 [38].

With the aim to construct novel nanostructured anode for high performance lithium ion microbattery, we developed a novel shell architecture TiO_2 as the negative material in this work. The material design is based on the fact that nano-structured TiO_2 with {001} facets can be deposited on the surface of polystyrene spheres (PS) functionalized by adsorption of polyelectrolytes [37], which is a water-soluble polymer containing ionizable groups and can provide polyanion and polycation to induce the nucleation of TiO_2. With the developed technology of PS assembly [39,40], we constructed the TiO_2-NCs into ordered monolayer spherical shells on a titanium foil, namely TiO_2-NCs/Ti electrode. This electrode has large specific surface areas, active facets and channel structures, which is essential for Li insertion/extraction and for Li^+-transport, hence delivering high-rate capability and high storage capacity.

2. Experimental

2.1. Materials synthesis

Based on the method of PS functionalization and the technology of templates assembly [37,40], a monolayer of sulfonated PS (s-PS) coated with polyelectrolytes was assembled on a glass substrate by confined convective assembly. Initially, this monolayer of s-PS was transferred onto a titanium foil ($5 \times 5 \times 0.127$ mm^3, 99.99%, Alfa Aesar) by a floating-transfer method. After being dried in air at room temperature, the substrate coated with a monolayer of s-PS was heated in an oven to 110 °C for 5 min, then immersed vertically in a freshly prepared liquid-phase deposition (LPD) solution (50 ml) containing $(NH_4)_2[TiF_6]$ (0.05 mol l^{-1}) and H_3BO_3 (0.15 mol l^{-1}). The pH value of the LPD solution was adjusted to 2.9 by adding HCl (2 mol l^{-1}) and the LPD solution was incubated at 50 °C for 8 h. After the reaction, the sample was washed with water and dried at room temperature, immersed in toluene (100 ml) to remove the PS templates, and calcined at 450 °C for 3 h in an oven under argon atmosphere.

To be able to estimate the mass of the deposited TiO_2 film, the number of the TiO_2-NCs spherical shells was determined, which was 9.5×10^{10} for a 5×5 mm^2 flat Ti substrate. Considering for 3D structures, a TiO_2-NCs spherical shell with 300 nm wall thickness and a density of 3.895 g cm^{-3}, the mass of deposited TiO_2 can be calculated. For a 5×5 mm^2 TiO_2 film, the mass of deposited TiO_2 is equal to 0.096 mg.

2.2. Materials characterization

The morphology of the sample was examined by field-emission scanning electron microscopy (FE-SEM; ZEISS Ultra 55, Germany) and transmission electron microscopy (TEM; JEM-2100HR, Japan). Crystallographic information for the sample was investigated with X-ray powder diffraction (XRD; Bruker D8 Advance, Germany). The surface area of the sample was measured using a Micromeritics ASAP 2020-physisorption analyzer (USA).

2.3. Electrochemical measurements

The electrochemical measurements were carried out using a coin-type cell (CR2025) with a metallic lithium foil as the counter and reference electrodes. The working electrode was the TiO_2-NC/Ti and the electrolyte was $LiPF_6$ (1.0 mol l^{-1}) in a 1:1 (w/w) mixture of ethylene carbonate (EC) and dimethyl carbonate (DMC). Cyclic voltammetry was conducted on a Solartron Analytical 1470E CellTest System (England) at different scanning rates and the charge/discharge tests were performed using a LAND CT2001A (China) battery testing system at different current rates with a voltage window of 1.0–3.0 V (*vs.* Li^+/Li).

3. Results and discussion

With our developed technology, a large area of titanium foil covered by functionalized s-PS (sulfonated polystyrene spheres) templates can be achieved easily. FE-SEM image (Fig. 1a) shows that the s-PS layer is flat and smooth, indicating that the template is a single layer, which ensures the formation of a monolayer of TiO_2 spherical shells. High-magnification FE-SEM (Fig. 1b) clearly reveals that the s-PS templates were assembled on a substrate of the titanium foil in arrayed monolayer successfully via a floating-transfer method. It is noteworthy that the polyelectrolytes adsorbed by s-PS play a key role during the process of self-organized TiO_2 on the surface of templates. As shown in Fig. 1, TiO_2 can hardly be organized on the surface of the bare s-PS (Fig. 1c). On the surface of the s-PS covered with the polyelectrolytes, however, well-defined and uniform TiO_2 layers can be successfully achieved (Fig. 1d). This result suggests that the deposition of TiO_2 using the LPD method is highly sensitive to a polyelectrolyte modification of the polymer surfaces, and the polyelectrolytes can induce the nucleation of TiO_2 on the surface of s-PS in the initial deposition. Moreover, TiO_2 were formed in nanocones and self-organized into 3D networks structure on the substrate, as shown in the inset of Fig. 1d.

Fig. 2 reveals the detailed features of the as-prepared samples. It can be seen from the side view (Fig. 2a) and the bottom view (Fig. 2b) that macroporous channels (red arrows in web version shown) were formed among spheres and between spheres and

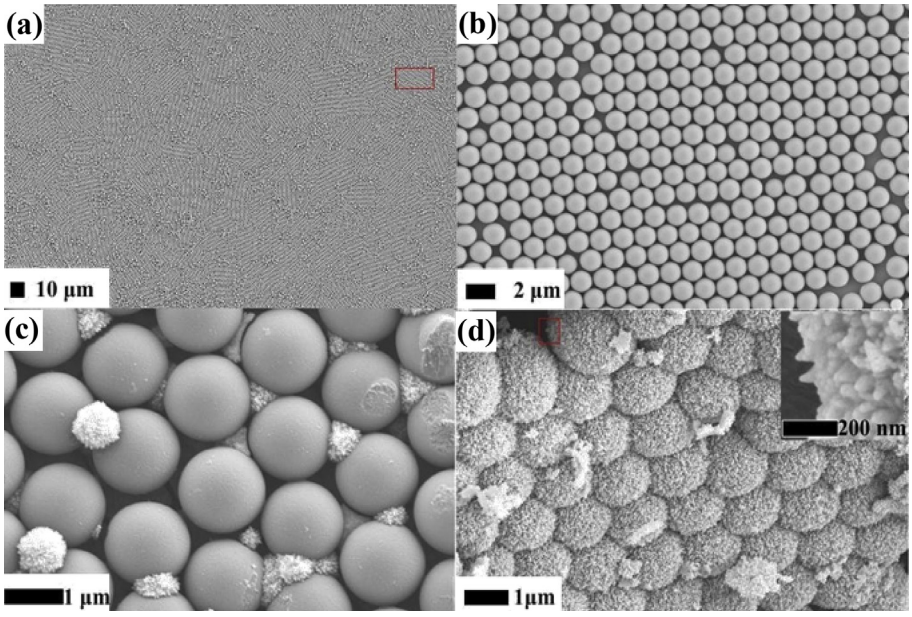

Fig. 1. FE-SEM images of s-PS templates (a, b) and self-organized nanoconic TiO_2 on the surface of templates (c, d).

the substrate due to the lack of TiO_2 growth. It can be expected that those channels help to improve the electrolyte transfer and enhance the reactivity of Li^+ insertion/extraction. These features can be confirmed by the electrochemical impedance spectroscopy (EIS) measurement (Fig. 3 and Table 1), which was performed on an electrochemical system (Autolab PGSTAT 30, Ecochemie, The Netherlands). The potential was set at 1.7 V, which is close to the OCP of a fresh cell. At this potential, the cell is in the state of full

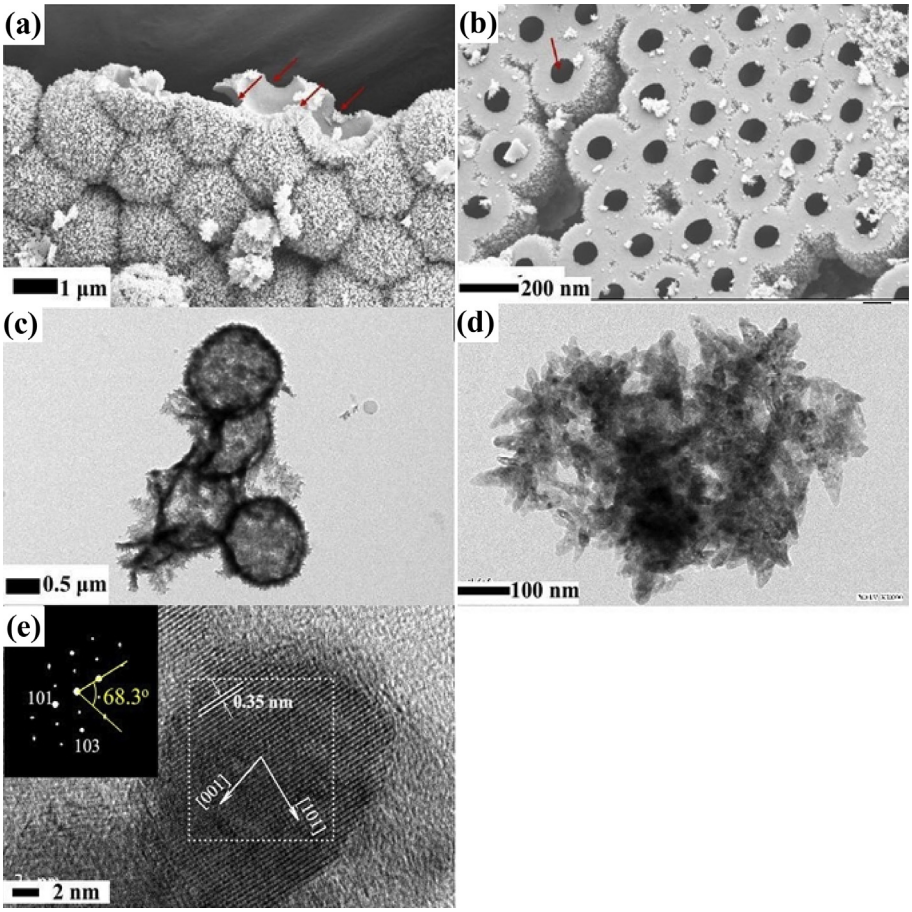

Fig. 2. FE-SEM images (a, side view; b, bottom view) and TEM image (c) of the TiO_2-NCs spherical shells; High-magnification TEM (d) of some debris of TiO_2-NCs spherical shells; High-resolution TEM image (e) recorded from single anatase TiO_2 nanocone and the corresponding fast-Fourier transform (FFT) pattern (the inset) of a single anatase TiO_2 nanocone.

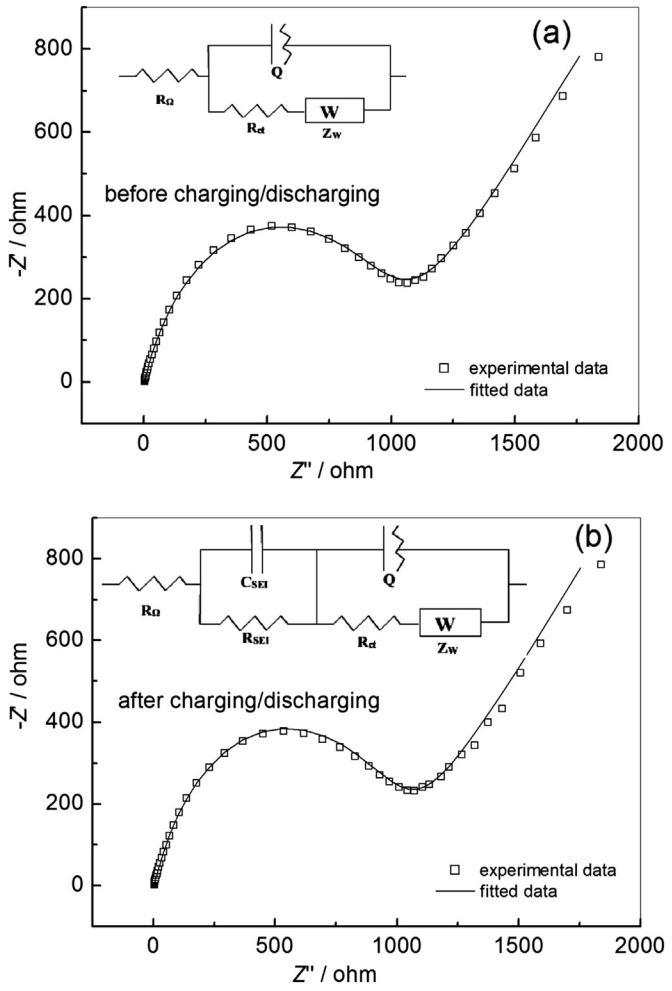

Fig. 3. Nyquist plots of the TiO_2-NCs/Ti electrode before (a) and after (b) the 5th charging/discharging and the equivalent circuits (inset).

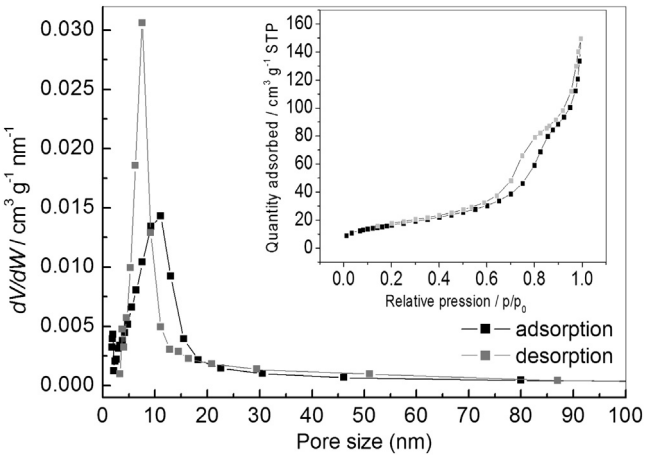

Fig. 4. The pore size distribution by Barrett–Joyner–Halenda (BJH) method from both branches of the nitrogen adsorption/desorption isotherm (inset) of the TiO_2-NCs spherical shells calcined at 450 °C for 3 h.

discharge. When EIS experiment is performed, a small potential disturbance is given, which should be accompanied with the lithium-ion insertion/extraction reaction. This potential was chosen for the measurement to reflect the state of working electrode, because the contribution of the counter electrode to the measured result might occur if other potentials were set. Fig. 3 shows the Nyquist plots together with the modeling results with the equivalent circuit (inset). In the equivalent circuit, R_Ω and R_{SEI} are associated with the resistance of electrolyte and SEI films, respectively, and R_{ct} is the charge-transfer resistance reflecting the reactivity of Li insertion/extraction in TiO_2. Z_W is the Warburg impedance representing the resistance from diffusion. It can be seen from Table 1 that R_Ω and R_{SEI} were too small compared to R_{ct} and Z_W, indicating that the electrode process is mix-controlled by charge-transfer and diffusion steps at these states. This result reveals the fact that the design of negative material with large area and channel structure is necessary and vital for the diffusion and insertion of Li^+ in TiO_2.

TEM image (Fig. 2c) shows that the wall thickness of the spherical shells is about 300 nm and the outer shell has a highly mesoporous nature, which is expected to have a large specific surface area. The Brunauer–Emmett–Teller (BET) measurement indicates that the surface area of the sample is 91.6 $m^2\ g^{-1}$ and the average pore size is 11.4 nm (Fig. 4), which are in great agreement with the TEM observations. The image (Fig. 2d) obtained from some debris of the TiO_2-NCs spherical shells clearly show the conic structure of TiO_2 and the network assembly of the TiO_2-NCs. Moreover, the length of the TiO_2-NCs can be easily obtained by Fig. 2d and the size is about 40–50 nm. It is expected that such a combination provide the electrode material with great porosity and thus improve the power density of the electrode via reducing the diffusion path length for ionic transport. The formation mechanism of the TiO_2-NCs has been understood in our previous work [37].

The HR-TEM image in Fig. 2e shows the anatase TiO_2 crystalline lattice fringes with an interplanar spacing of 0.35 nm, corresponding to anatase {101} facets. The XRD pattern (Fig. 5) also

Table 1
Impedance parameters of the TiO_2-NCs/Ti electrode before and after charging/discharging.

	R_Ω/Ω	R_{SEI}/Ω	R_{ct}/Ω	Z_W/Ω
Before	3.00	–	1020	847
After	3.33	7.70	995	862

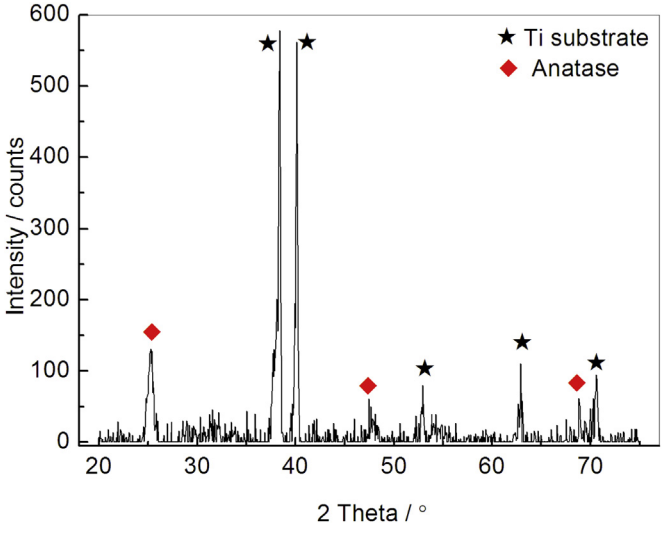

Fig. 5. XRD pattern of the TiO_2-NCs/Ti calcined at 450 °C for 3 h.

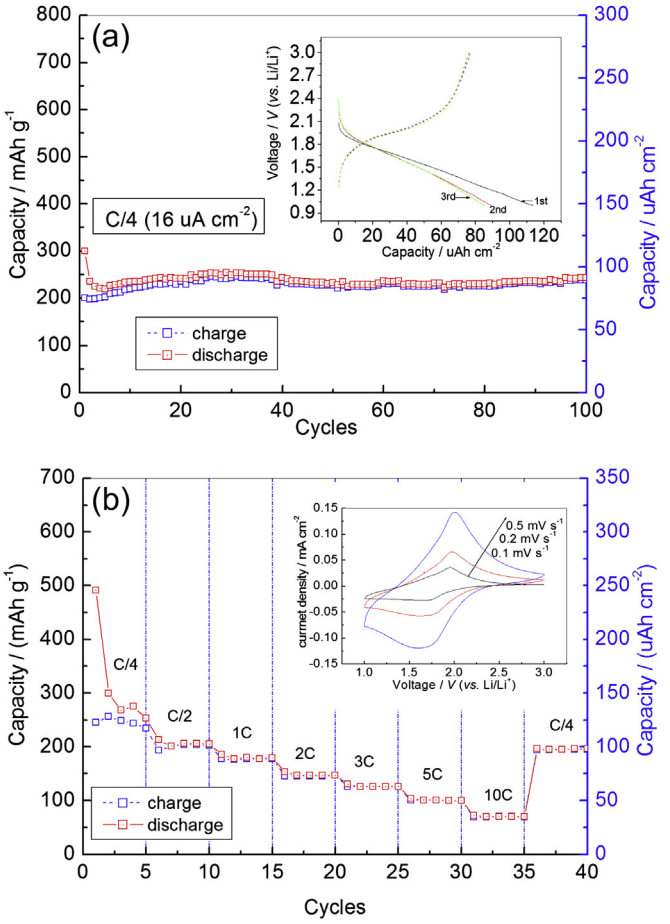

Fig. 6. Cycling performance (a) and rate capability (b) of the TiO_2-NCs/Ti electrode. All measurements are conducted with a voltage window of 1–3 V (*vs.* Li/Li^+).

confirmed that the TiO_2-NC only contain anatase except for the Ti substrate. Especially notable is the interfacial angle of 68.3° labeled in the corresponding fast-Fourier transform (FFT) pattern (Fig. 2e insert), which is identical to the theoretical value (68.3 ± 3°) for the angle between the {101} and {001} facets [41], suggesting that the TiO_2-NCs have exposed {001} facets on both the top and bottom of the nanocones. This preferred orientation is especially meaningful, because {001} facets possess superior Li storage capacity as described in the Introduction section.

The electrochemical performance of the TiO_2-NCs/Ti was evaluated by coin cells, and the obtained results are presented in Fig. 6. It can be seen from Fig. 6 that the TiO_2-NCs/Ti prepared in this work exhibits enhanced lithium storage properties and improved rate performance, compared to previously reported hollow TiO_2 nanostructures without the feature of ultra-small nanocones [38]. As shown in Fig. 6a, an initial discharge capacity as large as 298.9 mAh g^{-1} (113.6 μAh cm^{-2}) can be obtained and 242.1 mAh g^{-1} (92 μAh cm^{-2}) remains even after 100 cycles at 44.5 mA g^{-1} (C/4, 16 μA cm^{-2}), indicating that the TiO_2-NCs/Ti exhibits excellent cycling stability.

Fig. 7 shows the FE-SEM images of the TiO_2-NCs/Ti electrode before and after cycling. It can be seen that cycling the structure of materials was retained and the arrayed shells was not fractured after cycling, confirming the cycling stability of the TiO_2-NCs electrode.

The irreversible capacity loss in the initial cycle can be attributed to the formation of the SEI films [42] and the irreversible phenomena of lithium storage in the interface due to the large specific surface of the electrode materials [43]. The contribution of SEI can be confirmed by the EIS experiment. As shown in Fig. 3 and Table 1, although the SEI films were formed after the 5th cyclic test, R_{SEI} is small, only 7.70 Ω compared to the 995 Ω of R_{ct}. Another interesting result obtained from the EIS experiment is that the value of R_{ct} has scarcely changed before and after charging/discharging, meaning that the formation of the SEI films does not affect the reaction of Li insertion/extraction in TiO_2. Therefore, the good cycling stability and high Li storage of the TiO_2-NCs are mainly attributed to the inherent superiority of TiO_2, structural stability, and the ultra-small anatase TiO_2 with exposed {001} facets as well as its unique hierarchical structure and the spatial arrangement of the spherical shells. These features are vital for the stability, the safe operation and rate capability of LIBs.

Fig. 6b shows the rate capability of TiO_2-NCs/Ti electrode. The electrode delivers large lithium storage capacity at lower current rates. At C/4 (16 μA cm^{-2}) and C/2 (32 μA cm^{-2}), the specific discharge capacity of the TiO_2-NCs/Ti is ~250 mAh g^{-1} (115 μAh cm^{-2}) and ~204 mAh g^{-1} (100 μAh cm^{-2}), respectively. At higher current rates, large lithium storage capacity can be retained. When the current density increases to 5 C (320 μA cm^{-2}) and 10 C (640 μA cm^{-2}), the TiO_2-NCs/Ti still delivers ~100 mAh g^{-1} (~50 μAh cm^{-2}) and ~70 mAh g^{-1} (~35 μAh cm^{-2}), respectively. These values are far larger than those of other TiO_2 film electrodes [44].

The excellent rate performance is mainly due to the unique structure of the TiO_2-NCs. The highly porous channels and the high-energy facets help for the improvement of the conductivity of lithium ions and electrons, which weaken the polarization of the TiO_2-NCs. The small shift of peak potential observed from the cyclic voltammograms with scan rate (inset of Fig. 6b) confirms further these characteristics.

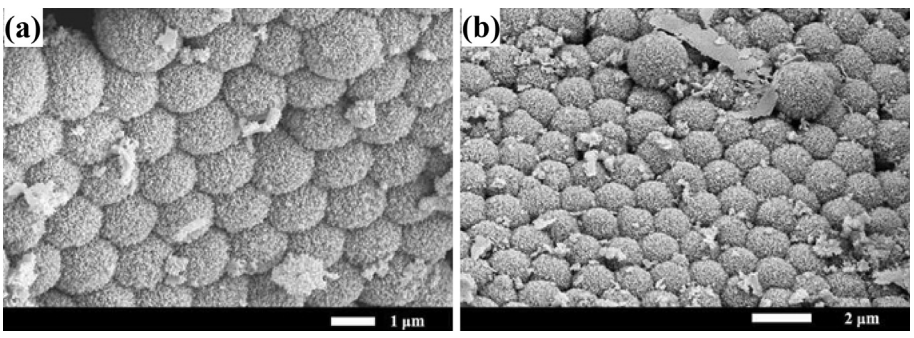

Fig. 7. FE-SEM images of the TiO_2-NCs/Ti electrode before cycle (a) and after 100 cycles of charging/discharging at 1 C.

4. Conclusions

Nano-architectured TiO_2-NCs electrode has been constructed as anode of lithium ion microbattery. The unique hierarchical structure of anatase TiO_2 with exposed {001} facets provides the high Li^+-transport channels and the high Li^+-reactivity facets, leading to the simultaneous improvement in electrochemical performance in terms of capacity, rate capability as well as cycling stability. The formed anatase TiO_2 nanocones with exposed {001} facets offer significant assistance for enhancing the lithium storage properties as well as the cyclic performance. The highly mesoporous and microporous nature offered by the architecture of TiO_2-NCs is responsible for the excellent rate performance.

Acknowledgments

This work is supported by the joint project of National Natural Science Foundation of China and Natural Science Foundation of Guangdong Province (Grant No. U1134002), National Natural Science Foundation of China (Grant No. 21273084), Natural Science Fund of Guangdong Province (Grant No. 10351063101000001), and the Key Project of Guangdong Province (Grant No. 20110110).

References

[1] C.L. Li, Q. Sun, G.Y. Jiang, Z.W. Fu, B.M. Wang, J. Phys. Chem. C 112 (2008) 13782–13788.
[2] J.W. Long, B. Dunn, D.R. Rolison, H.S. White, Chem. Rev. 104 (2004) 4463–4492.
[3] C.C. Li, Y.P. Zheng, T.H. Wang, J. Mater. Chem. 22 (2012) 13216–13222.
[4] H. Nakano, K. Dokko, J. Sugaya, T. Yasukawa, T. Matsue, K. Kanamura, Electrochem. Commun. 9 (2007) 2013–2017.
[5] P.J. Wojcik, A.S. Cruz, L. Santos, L. Pereira, R. Martins, E. Fortunato, J. Mater. Chem. 22 (2012) 13268–13278.
[6] P.G. Bruce, B. Scrosati, J.M. Tarascon, Angew. Chem. Int. Ed. 47 (2008) 2930–2946.
[7] H.Y. He, P. Zapol, L.A. Curtiss, Energy Environ. Sci. 5 (2012) 6196–6205.
[8] K. Xu, A.V. Cresce, J. Mater. Chem. 21 (2011) 9849–9864.
[9] M. Nathan, D. Golodnitsky, V. Yufit, E. Strauss, T. Ripenbein, I. Shechtman, S. Menkin, E. Peled, J. Microelectromech. Syst. 14 (2005) 879–884.
[10] W. Wang, M. Tian, A. Abdulagatov, S.M. George, Y.C. Lee, R.G. Yang, Nano Lett. 12 (2012) 655–660.
[11] Y.L. Wang, Q.L. Sun, Q.Q. Zhao, J.S. Cao, S.H. Ye, Energy Environ. Sci. 4 (2011) 3947–3950.
[12] J. Shen, B. Yan, M. Shi, H. Ma, N. Li, M. Ye, J. Mater. Chem. 21 (2011) 3415–3421.
[13] X.H. Liu, L.Q. Zhang, L. Zhong, Y. Liu, H. Zheng, J.W. Wang, J.H. Cho, Nano Lett. 11 (2011) 2251–2258.
[14] B. Liu, J. Zhang, X.F. Wang, G. Chen, D. Chen, C.W. Zhou, G.Z. Shen, Nano Lett. 12 (2012) 3005–3011.
[15] J. Pan, G. Liu, G.Q.M. Lu, H.M. Cheng, Angew. Chem. Int. Ed. 123 (2011) 2133–2137.
[16] X. Wang, G. Liu, L. Wang, J. Pan, G.Q.M. Lu, H.M. Cheng, J. Mater. Chem. 21 (2011) 869–873.
[17] Y. Dai, C.M. Cobley, J. Zeng, Y. Sun, Y. Xia, Nano Lett. 9 (2009) 2455–2459.
[18] Y.G. Guo, J.S. Hu, L.J. Wan, Adv. Mater. 20 (2008) 2878–2887.
[19] H.H. Lee, C.C. Wan, Y.Y. Wang, J. Electrochem. Soc. 151 (2004) A542–A547.
[20] J.C. Guo, X.L. Chen, C.S. Wang, J. Mater. Chem. 20 (2010) 5035–5040.
[21] Y. Yu, X. Wang, H. Sun, M. Ahmad, RSC Adv. 2 (2012) 7901–7905.
[22] D.Q. Zhang, G.S. Li, X.F. Yang, J.C. Yu, Chem. Commun. 0 (2009) 4381–4383.
[23] H.G. Yang, C.H. Sun, S.Z. Qiao, J. Zou, G. Liu, S.C. Smith, H.M. Cheng, G.Q. Lu, Nature 453 (2008) 638–641.
[24] G.N. Zhu, Y.G. Wang, Y.Y. Xia, Energy Environ. Sci. 5 (2012) 6652–6667.
[25] Y.C. Qiu, K. Yan, S.H. Yang, L.M. Jin, H. Deng, W.S. Li, ACS Nano 4 (2010) 6515–6526.
[26] H.G. Jung, S.W. Oh, J. Ce, N. Jayaprakash, Y.K. Sun, Electrochem. Commun. 11 (2009) 756–759.
[27] N. Lu, X. Quan, J.Y. Li, S. Chen, H.T. Yu, G.H. Chen, J. Phys. Chem. C 111 (2007) 11836–11842.
[28] A.L. Linsebigler, G. Lu, J.T. Yates, Chem. Rev. 95 (1995) 735–758.
[29] S.D. Senanayake, H. Idriss, Proc. Natl. Acad. Sci. U. S. A. 103 (2006) 1194–1198.
[30] M. Liu, L. Piao, L. Zhao, S. Ju, Z. Yan, T. He, C. Zhou, W. Wang, Chem. Commun. 46 (2010) 1664–1666.
[31] G. Liu, H.G. Yang, X. Wang, L. Cheng, J. Pan, G.Q. Lu, H.M. Cheng, J. Am. Chem. Soc. 131 (2009) 12868–12869.
[32] M. Liu, L. Piao, W. Lu, S. Ju, L. Zhao, C. Zhou, H. Li, W. Wang, Nanoscale 2 (2010) 1115–1117.
[33] E. Hosono, H. Matsuda, I. Honma, M. Ichihara, H. Zhou, Langmuir 23 (2007) 7447–7450.
[34] Y.W. Hu, T. Yang, X.X. Wang, K. Jiao, Chem. Eur. J. 16 (2010) 1992–1999.
[35] X. Han, Q. Kuang, M. Jin, Z. Xie, L. Zheng, J. Am. Chem. Soc. 131 (2009) 3152–3153.
[36] J. Yu, J. Fan, K. Lv, Nanoscale 2 (2010) 2144–2149.
[37] J.F. Lei, W.S. Li, X.P. Li, E.J. Cairns, J. Mater. Chem. 22 (2012) 22022–22027.
[38] J. Yi, D.S. Lu, X.P. Li, S.J. Hu, W.S. Li, J.F. Lei, Y. Wang, J. Solid State Electrochem. 16 (2012) 443–448.
[39] J.F. Lei, X.P. Li, W.S. Li, F.Q. Sun, D.S. Lu, J. Yi, Int. J. Hydrogen Energy 36 (2010) 8167–8172.
[40] J.F. Lei, X.P. Li, W.S. Li, F.Q. Sun, D.S. Lu, Y.L. Lin, J. Solid State Electrochem. 6 (2012) 625–632.
[41] G. Liu, C.H. Sun, H.G. Yang, S.C. Smith, L.Z. Wang, G.Q. Lu, H.M. Cheng, Chem. Commun. 46 (2010) 755–757.
[42] G. Sarre, P. Blanchard, M. Broussely, J. Power Sources 127 (2004) 65–71.
[43] J.F. Lei, K. Du, R.H. Wei, Jing Ni, L.B. Li, W.S. Li, RSC Adv., http://dx.doi.org/10.1039/C3RA41624K.
[44] Y.G. Guo, Y.S. Hu, W. Sigle, J. Maier, Adv. Mater. 19 (2007) 2087–2091.